Journal of Analytical and Applied Pyrolysis 104 (2013) 146–152

Contents lists available at ScienceDirect

Journal of Analytical and Applied Pyrolysis

journal homepage: www.elsevier.com/locate/jaap

Kinetic study of aspen during torrefaction

Jordan Klinger[a,b,*], Ezra Bar-Ziv[b], David Shonnard[a,c]

[a] Department of Chemical Engineering, Michigan Technological University, Houghton, MI 49931, USA
[b] Department of Mechanical Engineering-Engineering Mechanics, Michigan Technological University, Houghton, MI 49931, USA
[c] Sustainable Futures Institute, Michigan Technological University, Houghton, MI 49931, USA

ARTICLE INFO

Article history:
Received 17 April 2013
Accepted 22 August 2013
Available online 19 September 2013

Keywords:
Torrefaction
Kinetic modeling
Biocoal production
Thermal degradation

ABSTRACT

Using torrefied biomass, or biocoal, as a solid combustion fuel provides opportunity to introduce a sustainable feedstock into the energy market. The decomposition of biomass to biocoal is a very complex chemical process, yet detailed understanding of the mechanistic changes that occur can allow for system control and optimization. Torrefaction of lignocellulosic biomass has been studied extensively, and kinetic models have been developed to attempt to describe the observed behavior during Thermal Gravimetric Analysis (TGA) experiments, using very slow heating rates. The goal of this paper was to develop a baseline semi-empirical model for torrefaction of aspen wood using very fast heating rates (1000 °C/s) and GC–MS analysis. This fast heating rate was adopted in order to uncouple heat transfer and chemical kinetics.

Having direct information about the specific chemical evolution during torrefaction affords mechanistic insights into torrefaction, along with opportunities for improved process design and control. The proposed kinetics model involves three sequential reactions in which initially the parent hemicellulose material produces gaseous products (CO and CO_2), water, and organic acids (formic and acetic) and a solid intermediate. The next reaction further degrades the solid intermediate into the stated products. The final reaction further generates the products along with the final bio-coal product. We found the sequential reactions to have characteristic times of 0.99 min, 2.14 min and 39.45 min respectively at 300 °C. Improvements to the models and routes for future investigation are also discussed.

© 2013 Elsevier B.V. All rights reserved.

1. Introduction

Coal-fired utility boilers are the most prominent electricity generation systems, producing 40–50% of consumed electricity across the globe (42% in the U.S.) [1,2]. Coal exists in great abundance around the world, and is a valuable solid fuel because of its high energy density and low cost. Coal does, however, have well-know environmental issues such as the production of CO, CO_2, SO_x, NO_x, particulates, mercury, and poly-aromatic hydrocarbons to name a few [3–5]. In the current age of increasing environmental awareness, these issues inherent to coal combustion must be continuously addressed and controlled through the use of additional high-cost process operations.

A possible solution to environmental concerns is replacement of the coal by a different feedstock that is environment conscious–sustainable biomass. Because the coal-power industry is so prominent, it is important, if not necessary, to use a drop-in replacement in existing infrastructure. Initially, raw regenerative biomass was investigated as a possible solution, and demonstrated for commercial purposes [6,7]. The combustion of biomass inherently has a preferable emissions profile because it produces no net CO_2 emission due to a biogenic carbon cycle, and does not contain sulfur and mercury [8–11]. However, some issues exist with raw biomass processing and combustion, including high bulk volumes, moisture content, low calorific value, material hydrophobicity, production of undesirable tars, and high energy and time requirements for size reduction [12–14]. One solution to address these issues and still utilize biomass based fuel, has been the implementation of torrefaction as a pretreatment to produce biocoal.

Biomass torrefaction is a method of mild thermal treatment in the temperature range of 200–300 °C under inert atmosphere that, through a complex coupled chemical-kinetic-heat-and-mass-transfer process, converts the biomass into biocoal. In this process mostly the hemicellulose fraction of biomass degrades, with small contributions from the lignin and cellulose fractions [15–17]. The products of torrefaction are 70–90% solids (ash and biocoal), 6–35% liquid (mostly water with some fatty acids, phenols, acids, alcohols, furans, ketones) and 1–10% gas (CO, CO_2, H_2) [16,18].

There are major advantages to biocoal when compared to raw biomass, one of the most prominent being reduction in energy and time requirements for particle size reduction. The energy required

---

* Corresponding author at: Michigan Tech, 815 MEEM 1400 Townsend Drive, Houghton, MI 49931, USA. Tel.: +1 616 430 0941; fax: +1 906 487 2822.
E-mail address: jlklinge@mtu.edu (J. Klinger).

0165-2370/$ – see front matter © 2013 Elsevier B.V. All rights reserved.
http://dx.doi.org/10.1016/j.jaap.2013.08.010

Table 1
Ultimate and proximate analysis of coal, biocoal, and various raw biomass species [36–40].

Biomass	Ultimate analysis					Proximate analysis			
	C (%)	H (%)	O (%)	N (%)	S (%)	FC (%)	VM (%)	Ash (%)	HHV (MJ/kg)
Corn Stover [36]	42.6	5.1	36.5	0.8	0.1	15.4	69.7	6.9	16.3
Softwood [37]	52.1	6.1	41.0	0.2	0.0	28.1	70.0	1.7	20.1
Hardwood [37]	47.8	5.8	45.8	0.1	0.0	11.3	88.2	0.5	18.8
Switchgrass [36]	42.0	5.2	34.0	0.7	0.2	12.9	69.1	8.1	16.3
Lignite [37]	63.9	5.0	24.5	0.6	0.5	46.0	49.5	4.5	17.6
Sub-bit. Coal [38]	70.0	5.2	23.6	1.0	0.2	48.0	48.0	1.5	25.9
Biocoal [39,40]	70.7	5.6	20.1	0.6	–	32.3	63.5	1.9	28.5

FC: Fixed Carbon, VM: Volatile Matter, HHV: Higher Heating Value

to pulverize biocoal is approximately one tenth that of biomass [12]. This is due to the decomposition of hemicellulose which changes the viscoelastic properties of the feedstock [19]. In addition to this feedstock improvement, torrefaction also increases the calorific value of biomass up to 40% by removing bound feedstock moisture and reducing the mass by up to 30–50% [20,21]. Finally, the oxygen to carbon ratio is improved by significantly reducing the oxygen content, while the carbon fraction is increased accordingly [21]. Mostly importantly, torrefied biomass (biocoal) has similar physico-chemical properties to traditional coal and can be considered a premium drop-in replacement, requiring no addition upgrades to existing utility boilers. Table 1 compares the properties of coal, biocoal, and various raw biomass species.

Regardless of the feedstock or energy production method, however, a key aspect of electricity-generation systems is their high feedstock throughput [7,22]. As demands for energy are projected to increase consistently by approximately 50 quadrillion BTUs every 5 years starting from a measurement of 505 quadrillion BTUs in 2008 [23], a detailed understanding of the entire energy generation process is required for process optimization and design. Because of similarities between the properties of biocoal and traditional coal, most processing steps are similar to those already in practice with exception of feedstock production. For this reason among others, some emphasis has been placed into developing models and detailed understanding of the production of biocoal, or more specifically on torrefaction technology. Recent review articles have summarized several existing proposed wood torrefaction models based on Thermo Gravimetric Analysis (TGA) including a single step global model [24], a three parallel reaction Shafizadeh and Chin model [25], a two step consecutive Di Blasi–Lanzetta model [24,26,27], and a two parallel Broido–Shafizadeh model [24]. Despite these efforts there are many competing ideas about the complex chemical pathways, with no definite solution [17].

The present work focuses on proposing a mechanistic reaction scheme with a semi-empirical model, using different techniques than traditionally employed. The proposed models were developed with very high sample heating rates (1000 °C/s), and direct Gas Chromatography/Mass Spectroscopy (GC/MS) analysis. Very high heating rates during model development are critical in order to uncouple heat transfer from chemical reaction and thus study the true intrinsic reactions present during torrefaction.

2. Materials and methods

2.1. Biomass preparation

Debarked aspen samples were obtained from Dr. Christopher Webster in the School of Forest Resources and Environmental Science at Michigan Tech. Samples were debarked and then dried from their original moisture content at 105 °C in a drying oven until a difference in mass was no longer detectable. In addition, samples were milled to smaller particles using a small scale Thomas Wiley® knife mill (NR. 3557524 359264). Following size reduction, a W.S. Tyler Rotap (model RX-29, serial 9774) equipped with a range of sieve trays was used to obtain samples with known dimensions. Sizes larger than 32 Tyler Mesh (500 microns) but smaller than 28 Tyler

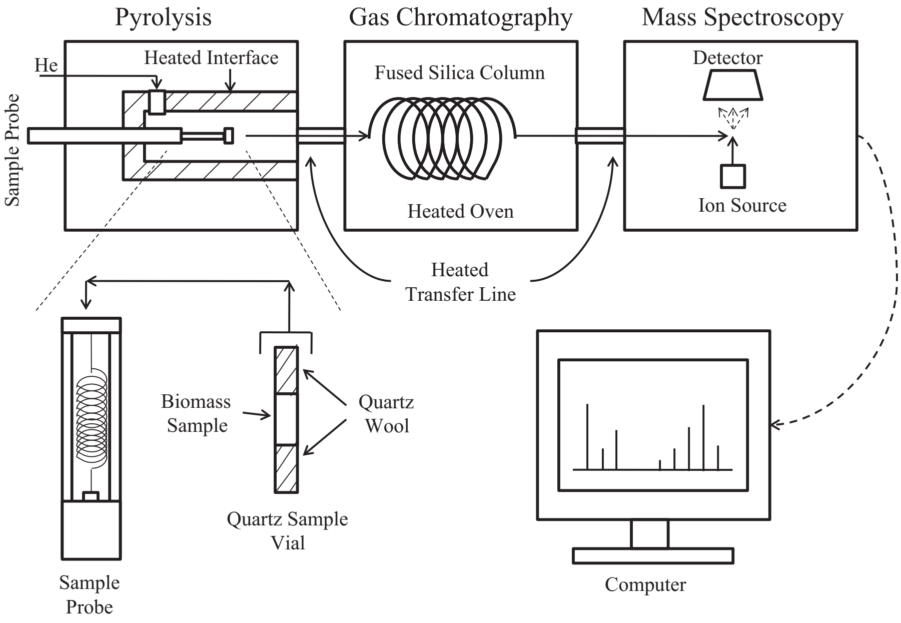

Fig. 1. Experimental flow diagram.

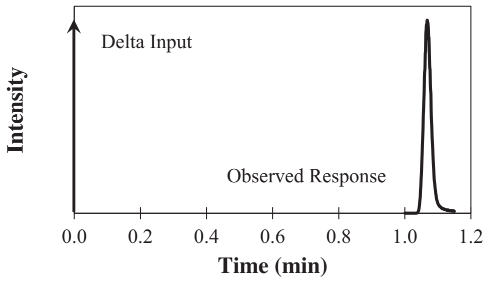

Fig. 2. Input-response diagram for acetic acid (60 *m*/*z*).

Mesh (599 microns) were considered for this study. The fibers were observed to have approximate shapes of cylinders. The wood fibers had diameter of approximately 0.5 mm and lengths ranging from 1.0–3.0 mm.

2.2. Torrefaction-GC/MS experiment

Torrefaction of aspen samples in this work was performed at 300 °C for 90 min with a micropyrolysis reactor (model 5200HP Pyroprobe) manufactured by CDS Analytical. A microbalance (Citizen Scales Inc., Model CM5) with a readability of 1 μg was used to record the sample masses. Fig. 1 shows the experimental apparatus.

During the experiment, approximately 0.5 mg biomass samples were contained within a quartz reaction vial with an inert ultra high pure (99.999%) helium atmosphere. Sample heating (1000 °C/s) is achieved via radiative, convective, and conductive heat transport from a platinum filament surrounding the transparent reaction vial. Once sample heating begins, the flow of helium gas over the sample is diverted to the inlet port on a Trace GC Ultra (Model K8880181) gas chromatograph by Thermo-Finnigan (now ThemoFisher) equipped with a 30 m RXI-5MS fused silica (low polarity phase, Crossbond® 5% diphenyl/95% dimethyl polysiloxane) capillary column by Restek. The GC column was maintained at 300 °C during experimental trials, and had a constant 1.5 ml/min (superficial velocity of 50.9 cm/s) gas throughout. The GC was connected to a quadrupole mass spectrometer (Trace DSQII, Thermo-Finnigan), which recorded the ion fragment intensities over time. The MS was set to monitor a range of molecular mass from 1–350 *m*/*z*. The experimental conditions mentioned above provided an environment that minimizes interactions of compounds with system components (GC column, etc.).

In addition to the experimental procedures above, great care was taken to evaluate complicating factors due to heat and mass transfer with the sample, column interaction effects, and flow dispersion. These evaluations combined both theoretical calculation and using pulse-inputs into the GC under conditions identical to the experiments. Input-response results are shown in

Fig. 2, and directly show how the instrument system interacts to create the observed signal. These results are discussed in the following sections.

3. Results and discussion

3.1. Method validation

The measurement of torrefaction products is affected by several factors. A complicating factor of great importance is limitations associated with heat transport. Using solutions for unsteady-state heat transfer in solids tabulated in work by Carslaw and Jaeger [28], it was found that approximately 90% of the surface temperature (boundary value) is observed by the center of a finite cylinder (with radius of the wood chips) after only 0.24 s. For these calculations the maximum effective radius (300 microns) allowable through the sieving step was considered for the characteristic length, along with a thermal diffusivity of 1.79 mm^2/s for biomass [29]. Detailed results and temperature profiles are shown in the supplemental material. Given that the time scale for conducting energy transport (0.24 s) is much less than the duration of the experiment (90 min), heat transfer limitations are considered to be very minor. The radiative heat transport from the heated filament to the biomass particle surface was not considered due to the effectiveness demonstrated in the slower of the two major heat transport steps, conduction.

Similar to the analysis addressing heat transport limitations, mass transport was investigated assuming a porous media model for the torrefied biomass. Using methods similar to heat transfer study, the transport is represented by an effective diffusion coefficient, and a value of 1.50 mm^2/s was assumed [30,31]. The mass transport becomes analogous to the heat transport, and in the case of torrefaction for the stated particle size mass transport limitations from diffusion is insignificant.

Finally, interactions of the products of torrefaction with the GC/MS instrumentation (GC column resin) were considered. An example of signal convolution due to the GC/MS is shown in Fig. 2 As indicated above in these tests, a GC auto sampler injects a sample (1 μl) of acetic acid at time zero; and this is represented by a delta function input. It is important to note that the amount of acetic acid injected was much greater than that observed over the time of torrefaction (90 min)–meaning that any observed interaction effects due to the system are accounted for liberally by this method. After approximately 62 s, the detector begins to observe a significant amount of the acetic acid ion fragment. Based on the superficial velocity, the time the gases/vapors take approximately 59 s to flow through the column. The output, or measured product signal, is dispersed in an almost Gaussian fashion, with a Full Width at Half Maximum (FWHM) of approximately 1.4 s. These results, when compared to the experiment duration of 90 min, indicate that there is negligible interaction with the chromatography system and the modeled compounds beyond the initial production

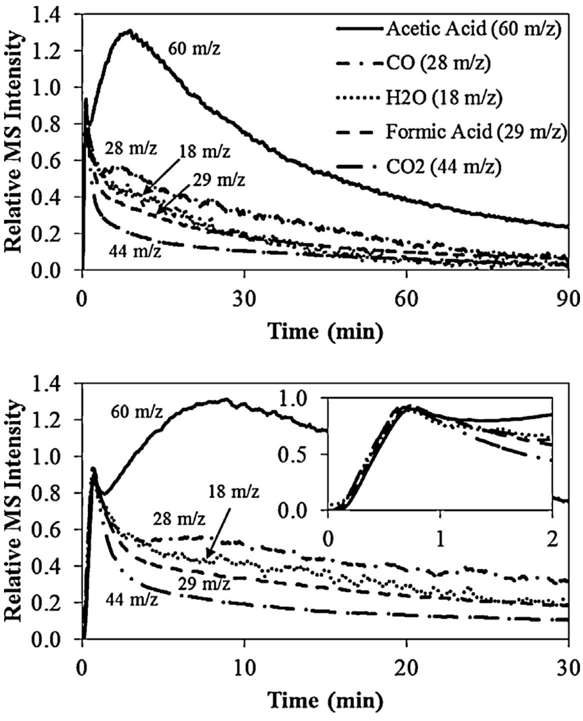

Fig. 3. (Top) Production rate of major compound ions over the full 90 min torrefaction experiment. (Bottom) The ion traces over the first 30 min of torrefaction. (Bottom Insert) Production rates over the first 2 min.

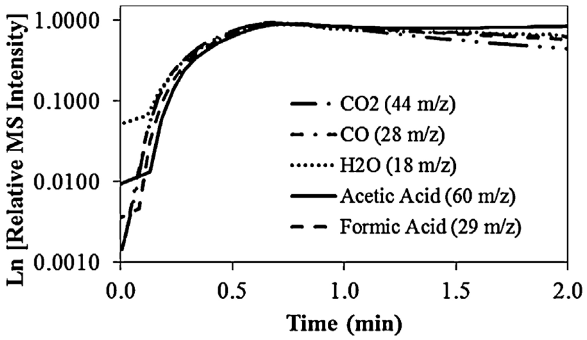

Fig. 4. Log-plot of compound production rates.

rate (<0.5 min). We conclude from these validation analyses that the measured response at the mass selective detector is indicating the actual rates of production of the species in the torrefaction chamber of the micropyrolysis instrument.

3.2. Model development

Although there are many identifiable compounds from torrefaction, the model in this work was targeted around major compounds produced during torrefaction, namely: CO, CO_2, water, and organic acids [21]. Fig. 3 shows a comparison between the MS relative intensities obtained for these compounds, represented by a characteristic ion fragment. The different plots represent the same data at varying time scales to highlight their similarities and differences – namely that their initial production are very similar, but several compounds exhibit a major secondary production peak. The characteristic fragments used were chosen based on their abundance in the species' fragmentation pattern: CO (28 m/z), CO_2 (44 m/z), water (18 m/z), acetic acid (60 m/z), and formic acid (29 m/z). Other species commonly associated with the 60 m/z fragment (glycolaldehyde and methyl formate) during thermal degradation were not detected, and are thought to originate from the decomposition of cellulose structure, which is not degraded significantly during torrefaction [32,33]. The carbonyl (29 m/z) fragment which is associated with a carboxyl group, was found to more readily form carboxylic acids as opposed to other organic compounds [21]. Finally, because 29 m/z was not observed as a characteristic ion fragment of acetic acid, this carbonyl fragment was associated directly to the other carboxylic acid detected, formic acid.

All compounds shown were normalized by the height of their *first* production peak for comparison (MS relative intensities), as some compounds exhibit more than one peak during torrefaction. The first production of all the compounds appears to be identical (characteristically) for all compounds at early times, though different as torrefaction advances. Examining these traces on a log-linear plot (Fig. 4) at early times (0.5–2.0 min) can aid in understanding the kinetics of production at early times. If relative intensity changes in a linear fashion when plotted as in Fig. 4, then the initial production is described by an exponential (first-order irreversible) decay process. From Fig. 4 if we exclude the first 0.5 min and focus on the behavior afterwards it is clear that these compounds are produced with similar characteristics (overlapping lines indicate the similar production) and with first order kinetics – i.e. they are produced simultaneously in the same first order reaction. From this, it is proposed that the first reaction in the torrefaction mechanism is the decomposition of the biomass hemicellulose to directly produce the various products. If this is true, the production rates must be at their maximum at time zero. This discrepancy with what is observed is caused by the small convolution imparted to the signal by heat-mass transfer as well as chromatographic influences previously discussed. It is proposed, then, that the first order exponential function that describes times 0.5–2.0 min should be extrapolated to describe the first reaction from time zero.

However, upon examining the production beyond these early times, it is noted that all compounds are continually produced yet with something other than a first order decay. Namely, the majority of acetic acid is produced beyond this first mechanism. The only way for this to occur is through the use of solid intermediates between the parent biomass and the final bio-coal. These intermediates would then further degrade to produce the observed species in subsequent irreversible first-order reactions. It is proposed that there are two additional reactions beyond the first, where solid intermediates produced from the previous reaction further degrade to produce the observed species.

3.3. Kinetic model and interpretation

The proposed set of reactions begins with the degradation of the parent hemicellulose material (H) into a solid reaction intermediate (R_1) and products from reaction 1 ($P_{i,1}$) with reaction rate constant k_1. The second reaction consists of the solid reaction intermediate further degrading through a second reaction rate constant (k_2) to further produce products ($P_{i,2}$) and intermediate (R_2). The third and final reaction produces products ($P_{i,3}$) and the final bio-coal product (C) from the second intermediate with rate constant (k_3). These reactions are summarized in Eqs. (1)–(3).

$$H \xrightarrow{k_1} R_1 + \sum_i \alpha_i P_i \tag{1}$$

$$R_1 \xrightarrow{k_2} R_2 + \sum_i \beta_i P_i \tag{2}$$

$$R_1 \xrightarrow{k_3} C + \sum_i \gamma_i P_i \tag{3}$$

where α_i, β_i, γ_i are stoichiometric coefficients for production of species i in reactions (1)–(3), and $k_1 > k_2 > k_3$. Assuming first order reactions, the time dependent solution for the rate of production of product P_i is shown in Eqs. (4)–(6), and the details of this solution are shown in the supporting materials.

$$\frac{dP_i}{dt} = \alpha_i k_1 H + \beta_i k_2 R_1 + \gamma_1 k_3 R_2 \tag{4}$$

$$\begin{aligned}
& & & \text{Contribution from} \\
\frac{dP_i}{dt} &= \alpha_i \theta \left[\exp(-k_1 t)\right] & & \text{(reaction1)} \\
&+ \beta_1 \theta \varphi \omega \left[\exp(-k_1 t) - \exp(-k_2 t)\right] & & \text{(reaction2)} \\
&+ \gamma_i \theta \varphi \omega \left[(k_2 - k_3)\exp(-k_1 t) + (k_3 - k_1)\exp(-k_2 t) - (k_2 - k_1)\exp(-k_3 t)\right] & & \text{(reaction3)}
\end{aligned} \tag{5}$$

$$\theta = k_1 H_0, \quad \varphi = \frac{k_2}{k_2 - k_1}, \quad \omega = \frac{k_3}{(k_3 - k_1)(k_2 - k_3)} \tag{6}$$

The reaction variables k_1, k_2, k_3, β_i, γ_i and $(H)_0$ were fit simultaneously to all data by minimizing the squared error between

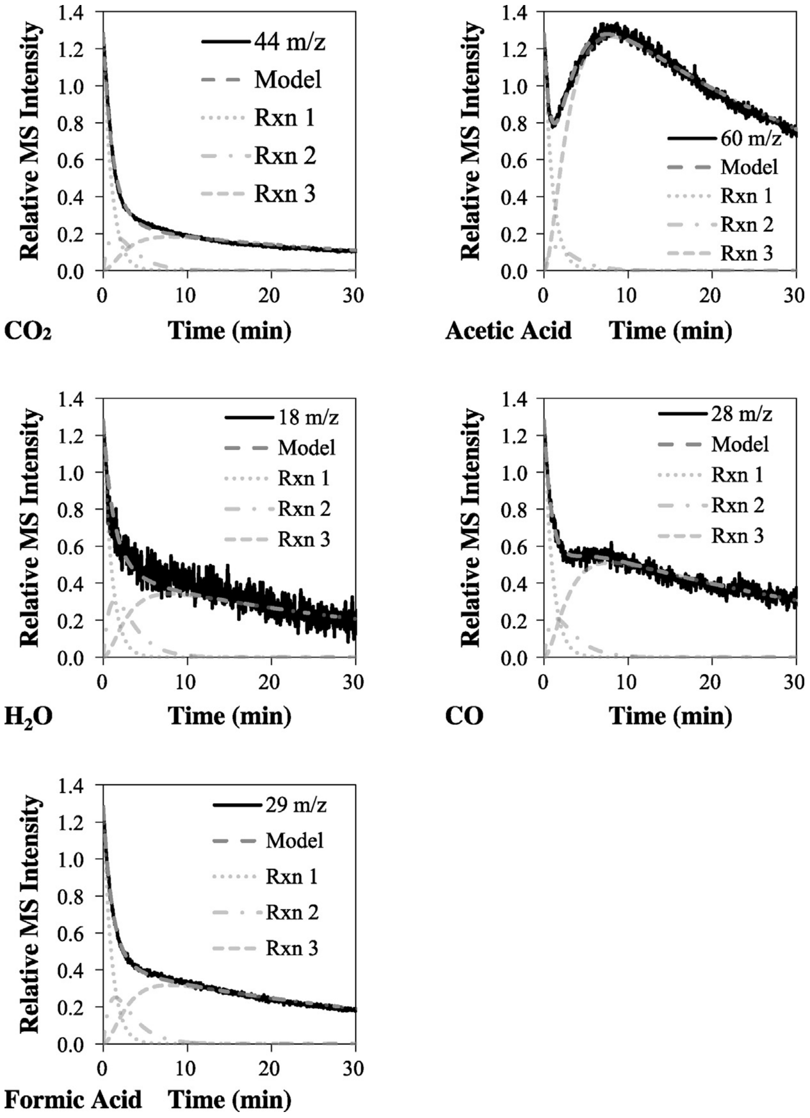

Fig. 5. Experimental rate data with model predictions.

the measured experimental data and the model predictions. The objective function to fit the variables is shown in Eq. (8).

$$\min \sum_{j} \sum_{j=0} \left(p_{i,j} - P_{i,j}\right)^2 \quad (8)$$

$$P_{i,j} = P\left(t_i, \left\{k_1, k_2, k_3, \beta_j, \gamma_j, (H)_o\right\}\right) \quad (9)$$

where $p_{i,j}$ is the measured data for species j at time i, $P_{i,j}$ is the calculated model value for species j at time i. The reaction rate coefficients were found to be $k_1 = 1.0079\ \text{min}^{-1}$, $k_2 = 0.4664\ \text{min}^{-1}$, and $k_3 = 0.0253\ \text{min}^{-1}$. The characteristic times, or inverse reaction rates, were 0.99 min, 2.14 min and 39.45 min respectively. The experimental data with the reaction scheme are shown in Fig. 5. This figure shows very close agreement between the proposed model (labeled "Model" in the figure) and the experimental data (labeled 44 *m*/*z*, 60 *m*/*z*, etc.), as well as the contributions from the three reactions (labeled "Rxn 1", "Rxn 2", "Rxn 3").

Each compound shares an identical production according to the first degradation reaction, which arises from the normalization of the data. During this method, α_i is forced to a value found with the extrapolation mention previously, while the other stoichiometric factors were calculated as relative values. The values of these coefficients are shown in Table 2. The model predicts that the maximum amount of hemicellulose occurs at time zero, while the first intermediate peaks around 1.5 min, and the second intermediate is maximized after approximately 8 min. It is clearly shown that the second reaction has some contributing effects, but the majority of sustained chemical production occurs during reaction 3. Perhaps the solid hemicellulose intermediate at this stage is unstable, or readily fragments to a more suitable derivative. For all species studied here, the model predictions are in good agreement with the laboratory data. This lends evidence to our proposed model, suggesting that the products are produced simultaneously is a series of sequential reactions. This idea is shared by other works which attempt to describe torrefaction. Table 3 displays a summary of some established torrefaction models [17].

Table 2
Stoicheometeric factors for each modeled compound.

	α_i	β_i	γ_i
CO	1.28	0.88	24.2
CO_2	1.28	0.78	8.65
H_2O	1.28	1.29	16.2
CH_3COOH	1.28	0.54	60.0
HCOOH	1.28	1.05	15.0

Table 3
Torrefaction kinetic models, adapted from [17,24,26,34,41].

Kinetic model	Mechanism scheme		Source
Three consecutive reactions	Hemicellulose	$\xrightarrow{k_1}$ Intermediate 1 + Volatile	*This work*
	Intermediate 1	$\xrightarrow{k_2}$ Intermediate 2 + Volatile	
	Intermediate 2	$\xrightarrow{k_3}$ Char + Volatile	
One step global	Hemicellulose	$\xrightarrow{k_1}$ Char + Volatile	[17,24]
Two consecutive parallel reactions	Hemicellulose	$\xrightarrow{k_1}$ Volatile $\xrightarrow{k_2}$ Intermediate	[26,34]
	Intermediate	$\xrightarrow{k_3}$ Volatile $\xrightarrow{k_4}$ Char	
Two parallel reactions	Hemicellulose	$\xrightarrow{k_1}$ Tars $\xrightarrow{k_2}$ Char + Volatile	[17,24]
Three parallel reactions	Hemicellulose	$\xrightarrow{k_1}$ Volatile $\xrightarrow{k_2}$ Tars $\xrightarrow{k_3}$ Char	[17]
Five parallel reactions (3 decomposition + 2 oxidation)	Hemicellulose	$\xrightarrow{k_{1,2,3}}$ $\text{Volatile}_{1,2,3}$ $\xrightarrow{k_{4,5}}$ $\text{Volatile}_{4,5}$	[41]

When compared to existing models, the work here has several novel aspects and insights: (1) moves beyond lumped models, to the identification of specific chemical species transients' during torrefaction, (2) the model was developed around observed species, and thus direct changes to the biomass instead of weight loss curves, (3) very fast heating rates, which decoupled transport and kinetic effects arising from temperature ramping. When comparing to existing models, perhaps the closest match is the two-step consecutive Di Blasi–Lanzetta model. This model has been used extensively in other studies in attempt to explain trends obtained from TGA studies [26,34,35]. In this model, the parent biomass (A) forms volatile product group 1 (V_1) and a reaction intermediate (B) through reaction rates k_{v1} and k_1 respectively. After this first reaction, the intermediate is further broken into a second group of volatile products (V_2) and a solid product (C). These reactions are summarized in Eqs. (10)–(11) [26].

$$A\xrightarrow{k_{v1}}V_1,\ A\xrightarrow{k_{v1}}B \tag{10}$$

$$B\xrightarrow{k_{v2}}V_2,\ B\xrightarrow{k_2}C \tag{11}$$

4. Conclusions and recommendations

The new model presented in this work describes the evolution of gases (CO and CO_2), water, and organic acids (formic and acetic) from the torrefaction of aspen. The proposed models were formed around the observations of fast product evolution followed by varying amounts of sustained production at later times. The model consists of three sequential reactions with characteristic times of 0.99 min, 2.14 min and 39.45 min respectively. The data for the species measured were well fit by the model. Transient characterization of the remaining biomass solids could provide a well-defined path for model improvements. Techniques such as Fourier transform infrared spectroscopy (FTIR) could be employed to develop a key understanding of change in functional groups. In addition, convoluting factors such as heat transfer, flow dispersion, and GC column interaction should be further addressed or incorporated in the model to further refine the key early-time assumptions.

Appendix A. Supplementary data

Supplementary data associated with this article can be found, in the online version, at http://dx.doi.org/10.1016/j.jaap.2013.08.010.

References

[1] EIA, *Report #: DOE/EIA*-0484, (2009).
[2] EIA, Report #: DOE/EIA-0383, (2010).
[3] W.S. Smith, C.W. Gruber, Public Health Service Publication; (United States), vol. 999-AP-24, 1966, Medium: X; Size: Pages: vp.
[4] Y. Zhao, S. Wang, L. Duan, Y. Lei, P. Cao, J. Hao, Atmospheric Environment 42 (2008) 8442.
[5] A.M. Mastral, M.S. Callén, T. Garcia, Fuel Processing Technology 67 (2000) 1.

[6] D. Ayhan, Energy Policy 36 (2008) 834.
[7] J.P. Reichling, F.A. Kulacki, Energy 36 (2011) 6529.
[8] M.M. Wright, R.C. Brown, A.A. Boateng, Biofuels, Bioproducts and Biorefining 2 (2008) 229.
[9] C.M. Gasol, X. Gabarrell, A. Anton, M. Rigola, J. Carrasco, P. Ciria, J. Rieradevall, Biomass and Bioenergy 33 (2009) 119.
[10] J. Fan, T.N. Kalnes, M. Alward, J. Klinger, A. Sadehvandi, D.R. Shonnard, Renewable Energy 36 (2011) 632.
[11] R. Saidur, E.A. Abdelaziz, A. Demirbas, M.S. Hossain, S. Mekhilef, Renewable and Sustainable Energy Reviews 15 (2011) 2262.
[12] P.C.A. Bergman, ECN Biomass, DEN Programme of SenterNovem, Dutch Ministry of Economic Affairs, Report ECN-C-05-073, 2005.
[13] L. Devi, K.J. Ptasinski, F.J.J.G. Janssen, Biomass and Bioenergy 24 (2003) 125.
[14] M.J. Prins, K.J. Ptasinski, F.J.J.G. Janssen, Energy 32 (2007) 1248.
[15] H. Yang, R. Yan, H. Chen, D.H. Lee, C. Zheng, Fuel 86 (2007) 1781.
[16] R.D. Boardman, J.R. Hess, S. Sokhansanj, J.S. Tumuluru, C.T. Wright, Industrial Biotechnology 7 (2011) 384.
[17] J.J. Chew, V. Doshi, Renewable and Sustainable Energy Reviews 15 (2011) 4212.
[18] D. Ciolkosz, R. Wallace, Biofuels, Bioproducts and Biorefining 5 (2011) 317.
[19] A.J. Panshin, C. deZeeuw, Textbook of Wood Technology, McGraw-Hill Book Company, New York, 1980.
[20] W.-H. Chen, H.-C. Hsu, K.-M. Lu, W.-J. Lee, T.-C. Lin, Energy 36 (2011) 3012.
[21] M.J.C. van der Stelt, H. Gerhauser, J.H.A. Kiel, K.J. Ptasinski, Biomass and Bioenergy 35 (2011) 3748.
[22] P.L. Spath, M.K. Mann, D.R. Kerr, National Renewable Energy Laboratory, Golden, Colorado, 1999.
[23] DOE/EIA, U.S. Energy Information Administration, 2011.
[24] V. Repellin, A. Govin, M. Rolland, R. Guyonnet, Biomass and Bioenergy 34 (2010) 602.
[25] F. Shafizadeh, P.P.S. Chin, Wood Technology: Chemical Aspects ACS symposium series, American Chemical Society, 1977, pp. 57 (Chapter 5).
[26] C. Di Blasi, M. Lanzetta, Journal of Analytical and Applied Pyrolysis 40–41 (1997) 287.
[27] M.J. Prins, K.J. Ptasinski, F.J.J.G. Janssen, Journal of Analytical and Applied Pyrolysis 77 (2006) 28.
[28] H.S. Carslaw, J.C. Jaeger, Conduction of heat in Solids, 2nd ed., Clarendon Press, Oxford, 1959.
[29] B.V. Babu, A.S. Chaurasia, Energy Conversion and Management 45 (2004) 53.
[30] F. He, F. Behrendt, Combustion and Flame 158 (2011) 2500.
[31] C. Di Blasi, Chemical Engineering Science 51 (1996) 1121.
[32] R.J. Evans, T.A. Milne, Energy and Fuels 1 (1987) 123.
[33] P.R. Patwardhan, J.A. Satrio, R.C. Brown, B.H. Shanks, Journal of Analytical and Applied Pyrolysis 86 (2009) 323.
[34] R.B. Bates, A.F. Ghoniem, Bioresource Technology 124 (2012) 460.
[35] A. Pétrissans, R. Younsi, M. Chaouch, P. Gérardin, M. Pétrissans, Journal of Thermal Analysis and Calorimetry 109 (2012) 907.
[36] J.S. Tumuluru, S. Sokhansanj, C.T. Wright, R.D. Boardman, N.A. Yancey, ASABE Annual International Meeting, 2011, Louisville, Kentucky.
[37] J. Parikh, S.A. Channiwala, G.K. Ghosal, Fuel 84 (2005) 487.
[38] D.H. Ahn, B.M. Gibbs, K.H. Ko, J.J. Kim, Fuel 80 (2001) 1651.
[39] A. Demirbaş, Energy Conversion and Management 42 (2001) 1229.
[40] T.G. Bridgeman, J.M. Jones, A. Williams, D.J. Waldron, Fuel 89 (2010) 3911.
[41] M. Broström, A. Nordin, L. Pommer, C. Branca, C. Di Blasi, Journal of Analytical and Applied Pyrolysis 96 (2012) 100.